Mechanical and hydraulic characterization of plastic concrete for seepage cut-off walls

S. Hinchberger, J. Weck, and T. Newson

Abstract: This paper describes a series of laboratory tests performed to characterize the mechanical and hydraulic properties of plastic concrete (PL-C). PL-C is used in the construction of seepage cut-off walls in dams and it comprises cement, aggregate, and water mixed with sodium bentonite. The addition of sodium bentonite causes a reduction in strength and improved ductility after failure compared with normal concrete. The mechanical properties of PL-C are studied using a series of unconfined compression tests and confined compression tests performed while simultaneously permeating water through PL-C specimens. Stress relaxation and controlled rate of loading tests are also performed to investigate the rate-sensitivity and time-dependency of plastic concrete. The test results show that the hydraulic conductivity of PL-C increases between two and three orders of magnitude during triaxial compression due to yielding, crack formation, and dilation of the cracks. Such changes in the behaviour of PL-C should be minimized during design by controlling the working strains and using erosion-resistant mixes. In addition to these findings, PL-C exhibits significant time-dependent behaviour similar to that observed for clays, and the variation of compressive strength versus confining stress is comparable to normal strength concrete.

Key words: plastic concrete, stress relaxation, hydraulic conductivity, axial strain, dams.

Résumé : Cet article décrit une série d'essais en laboratoire effectués dans le but de caractériser les propriétés mécaniques et hydrauliques du béton plastique (BP). Le BP est utilisé dans la construction de systèmes de coupure dans les barrages. Il est constitué du ciment, de l'agrégat et de l'eau mélangé avec de la bentonite de sodium. L'ajout de bentonite de sodium entraîne une réduction de la résistance et une amélioration de la ductilité suite à la rupture, comparativement au béton standard. Les propriétés mécaniques du BP sont étudiées à l'aide d'essais en compression non confinés et confinés effectués en même temps que l'eau pénètre à travers les échantillons de BP. Des essais de relaxation des contraintes et de chargement à taux contrôlé ont aussi été effectués pour investiguer la sensibilité au taux et la dépendance au temps des BP. Les résultats des essais montrent que la conductivité hydraulique du béton plastique augmente de deux à trois ordres de grandeur durant la compression triaxiale en raison de l'écoulement, de la formation de fissures et de la dilatation dans les fissures. Ces changements dans le comportement du BP devraient être minimisés durant la conception par un contrôle des déformations et par l'utilisation de mélanges résistants à l?érosion. De plus, le béton plastique démontre un comportement dépendant du temps de façon significative, comme ce qui est observé pour les argiles, et la variation de la contrainte compressive versus la contrainte de confinement est comparable à la résistance normale d'un béton.

Mots-clés : béton plastique, relaxation des contraintes, conductivité hydraulique, déformation axiale, barrages.

[Traduit par la Rédaction]

Introduction

Advancements in the construction of plastic concrete (PL-C) cut-off walls have enabled the construction of large zoned earthfill embankment dams on deep pervious foundations (Davidson et al. 1992; Balian 2007). In some cases, PL-C cut-off walls have also been used to rehabilitate aging structures (e.g., Rigbey 2006). PL-C comprises a mixture of cement, water, aggregate, and bentonite, which has low hydraulic conductivity and excellent ductility after reaching failure compared with conventional concrete. Figure 1 shows typical normalized stress–strain curves for conventional concrete and PL-C.

The primary function of a PL-C cut-off wall is to control or eliminate foundation seepage below dams from upstream to downstream. For dams that require a foundation cut-off, the cut-off wall is typically constructed in the foundation by the slurry trench method, then the dam is built on top of the cut-off wall and foundation. Figure 2 shows the typical geometry. During embankment construction, both the foundation and PL-C compress under the weight of the earthfill structure. Consequently, the PL-C may undergo significant plastic straining potentially leading to (*i*) cracking and (*ii*) an increase in the hydraulic conductivity. Increases in the hydraulic conductivity of PL-C can reduce the hydraulic efficiency of a cut-off wall and affect the distribution of the piezometric head downstream of the wall; cracking can make the wall susceptible to hydraulic erosion (Davidson et al. 1992). So far, the influence of compressive strain on the

Received 18 September 2007. Accepted 25 August 2009. Published on the NRC Research Press Web site at cgj.nrc.ca on 7 April 2010.

S. Hinchberger[1] and T. Newson. Department of Civil and Environmental Engineering, The University of Western Ontario, London, ON N6A 5B9, Canada.
J. Weck. Hatch Energy, 4342 Queen Street, Niagara Falls, ON L2E 6W1, Canada.

[1]Corresponding author (e-mail: shinchberger@hatch.ca).

Fig. 1. Stress–strain response of normal strength concrete compared with plastic concrete. σ_{axial}, axial stress; σ_{peak}, peak stress at failure.

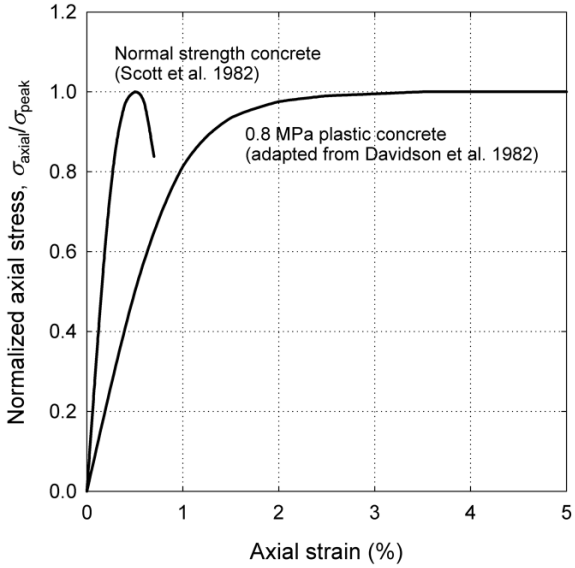

hydraulic conductivity of PL-C has not been reported in the literature.

This paper describes a series of unconfined compression tests and triaxial compression tests with simultaneous hydraulic conductivity measurements that were performed to characterize the mechanical and hydraulic properties of PL-C. PL-C specimens were prepared from three different concrete mixes and cured for at least 28 days to achieve unconfined compressive strengths (f_{cu}) ranging from 0.65 to 2.5 MPa. The specimens were compressed to failure at confining pressures (σ_c) ranging from 0 to 100, 400, and 900 kPa. During the confined tests ($\sigma_c \neq 0$), compression was halted at axial strains (ε_a) of 0.5%, 1%, 2%, 4%, 6%, 8%, and 10% and ε_a was held constant while water was simultaneously permeated through the specimens. These tests were used to characterize the influence of strain on the hydraulic conductivity of PL-C and study the stress-relaxation of PL-C during periods of constant strain. The primary objectives of this paper are to (*i*) describe an approach to measure the effect of ε_a during triaxial compression on the hydraulic conductivity of PL-C, (*ii*) characterize the effects of time and compression rate on the response of PL-C, and (*iii*) characterize the effect of ε_a on the hydraulic conductivity of PL-C. The results of this study are considered to be of interest to geotechnical engineers and dam engineers.

Methods and materials

Materials

The PL-C mixes prepared in this study were batched using type 10 Portland cement (PC). Sodium (Na) bentonite (Halliburton–Quik Gel) was added to the PC, aggregate, and water as described below to create PL-C. The specific gravity, liquid limit, and plastic limit of the Na–bentonite are 2.75, 570%, and 52%, respectively. Both fine and coarse aggregates were used in the PL-C mixes. Figure 3 shows the gradation curves for coarse and fine aggregates. The maximum aggregate size was 12 mm, which is acceptable for the 75 mm diameter specimens prepared for use in this study (see Issa et al. 2000).

Batching methods

Initially, PL-C mix proportions corresponding to f_{cu} of 0.65, 0.9, and 2.5 MPa were estimated using design charts from the U.S. Army Corps of Engineers (Kahl et al. 1991). However, some adjustments to the water to cement ratio (*w*:*c*) were required as described below. The following describes the batching process.

First, fine and coarse aggregates were spread out on a concrete floor and air-dried at room temperature (21 °C) for at least 24 h. Simultaneously, water and Na–bentonite were blended together in a 10 L plastic container using a high-speed mixer until a smooth and consistent slurry was achieved. Then the bentonite–water slurry was allowed to hydrate for 24 h. After 24 h, the fine and coarse aggregates were placed in a concrete mixer (Stow, Model CMC65) and mixed for 5 min to ensure adequate blending of the aggregates. Then, type 10 PC was added to the mixer and blended with the aggregate for 3 min. Lastly, the slurry (bentonite plus water) was added and the entire batch was mixed until a uniform consistency was achieved. Table 1 lists the slurry density.

Typically, PL-C is placed by the tremmie method. For this placement method, the concrete slump must be at least 200 mm (Kahl et al. 1991). Consequently, prior to casting the PL-C specimens, a slump test was done according to ASTM C143 (ASTM 1998*a*). If the slump was less than 200 mm, additional slurry was added to the mixer until 200 to 225 mm slump was achieved.

After mixing and adjusting the slump, PL-C was placed into 75 mm × 150 mm plastic cylinder moulds without prodding or vibrating. As such, the results presented in this paper correspond to the behaviour of PL-C cured at negligible confining stresses; whereas the in situ confining stresses are significantly higher. This will be discussed at the end of the paper. The specimens were immediately placed in a wet room to cure for a minimum of 28 days and a maximum of 65 days. Specimens were taken from the wet room on the third day after casting, removed from the plastic cylinder moulds, and then returned to the wet room. 75 mm × 150 mm (diameter to height) specimens were used in this study due to limitations of the axial load cell used with the triaxial compression machine (25 kN maximum load).

Batch proportions

In total, 26 PL-C specimens were prepared from three separate batches for compression testing. As noted above, the initial batch proportions were estimated from Kahl et al. (1991) and then adjusted by adding additional slurry to give a slump between 200 and 225 mm. Table 1 summarizes the final mix proportions after adjustments for the slump and Table 2 summarizes the specimens. It is noted that for PL-C (*i*) *w*:*c* is the mass of water divided by the mass of cement plus Na–bentonite and (*ii*) the bentonite content is the mass of Na–bentonite divided by the mass of Na–bentonite plus cement expressed as a percent (Kahl et al. 1991). In addition, as shown in Table 1, the density of the slurries during mixing varied from 1.052 g/cm^3 for batch

Fig. 2. Typical dam geometry with cut-off wall (cross section).

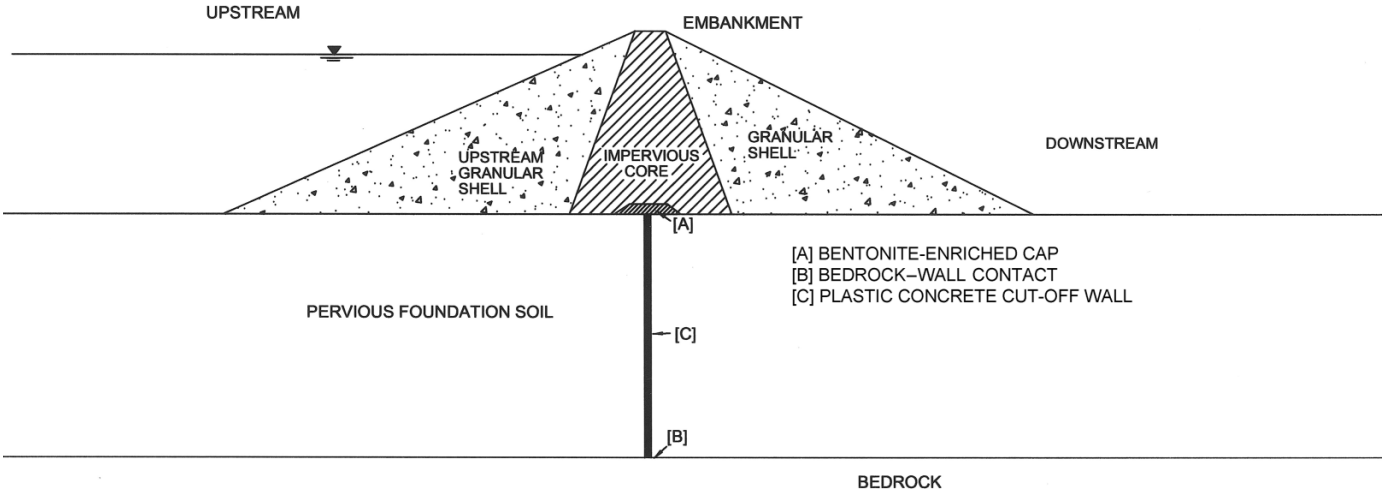

Fig. 3. Grain size of concrete aggregates.

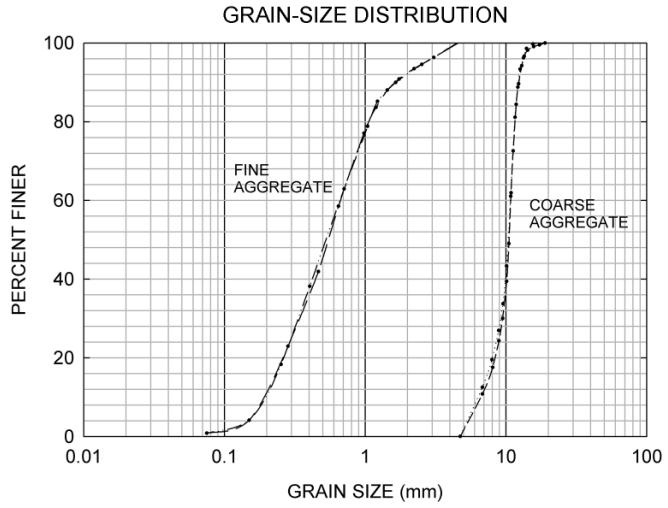

B2 to 1.071 g/cm^3 for batch B1, which are near the upper range used in situ (e.g., Soroush and Soroush 2005). As such, the test results presented in this paper correspond to the behaviour of PL-C mixes with a high bentonite content and relatively high ductility.

Finally, the additional slurry added to the PL-C batches to adjust the slump caused a 35%–41% reduction in f_{cu} compared with the design charts (Kahl et al. 1991). The amount of reduction of f_{cu} (measured versus design) is shown in the last column of Table 1. Discrepancies in the slump, f_{cu}, and w:c ratios in this study compared with those in Kahl et al. (1991) can be attributed to differences in properties of the bentonite used herein, such as the dielectric constant, specific surface, and cation exchange capacity. Also, as noted by Hutchinson et al. (1975), the method of mixing and hydrating bentonite slurry can affect the slurry rheology and have some effect on the f_{cu}.

Testing and procedures

This section describes the tests and procedures used to characterize the mechanical and hydraulic properties of PL-C. As noted above, Table 2 summarizes the test speciments.

Unconfined compression tests

The f_{cu} of PL-C was measured in accordance with ASTM standard D2166 (ASTM 2005) using either (*i*) a 90 tonne Avery compression machine or (*ii*) a Global Digital Systems (GDS) computer controlled triaxial system similar to that described by Menzies (1988). For each of the PL-C batches listed in Table 1, three unconfined compression tests were performed using a compression rate of 0.012 mm/min: two tests were performed using the Avery compression machine on specimens with sulfur end caps prepared according to ASTM standard C617 (ASTM 1998*b*) and one test was performed using the GDS triaxial system on specimens that were cut using a diamond blade rock saw to achieve flat orthogonal ends. The purpose was to assess if the saw cut ends had an effect on f_{cu}.

For unconfined compression tests performed using the GDS apparatus, axial strain (ε_a) was measured using the following two methods:

(1) A linear voltage displacement transducer (LVDT) was mounted on the load frame so that it came to rest on the triaxial cell and ε_a was deduced from the relative displacement between the load frame and triaxial cell. Such an approach gives the global strain neglecting compression of the porous stones, load cell, and load cap.

(2) Strain gauges were bonded to the specimens to measure local axial strain during compression.

The strains obtained using methods (1) and (2) were within 0.1% for loads up to 15 kN as shown in Table 3.

Triaxial compression and hydraulic conductivity tests

A series of triaxial compression tests were performed on PL-C specimens using the GDS computer-controlled triaxial system (Menzies 1988), which allowed constant rate of strain (CRS) loading in compression and simultaneous hydraulic conductivity measurement. These tests were performed using confining pressures (σ_c) of 100, 400, and 900k Pa and top and bottom cap pressures of 65 and 55 kPa, respectively, as summarized in Table 2. The range of σ_c used during these tests was established from a series of finite element analyses and it corresponds to the range of lateral confining pressure acting in situ on a PL-C cut-off

Table 1. Plastic concrete mix proportions.

Batch	Cement factor* (kg/m^3)	Bentonite content† (%)	Slurry density (g/cm^3)	*w*:*c* ratio‡	Fine:coarse aggregate ratio	f_{cu} (MPa)	$f_{cu}/f_{cu\text{-}d}$
B1	166	30	1.071	2.25	1:1	0.6	0.60
B2	130	20	1.052	2.35	1:1	0.95	0.59
B3	214	20	1.068	1.7	1:1	2.5	0.65

Note: f_{cu} and $f_{cu\text{-}d}$, measured and design compressive strength, respectively.
*Bentonite and cement by mass per cubic metre of PL-C.
†Percent bentonite by mass in the cement factor.
‡Ratio of water to cement plus bentonite by mass.

Table 2. Test specimens.

Specimen*	Age (days)†	Apparatus	σ_c (kPa)	Permeation pressures (kPa)		Test type	Compressive strength (MPa)	
				Top	Bottom		0.012 mm/min	8 h relaxed
B1-1	28	A	0	—	—	UC_{SC}	0.62	—
B1-2	28	A	0	—	—	UC_{SC}	0.66	—
B1-3	28	GDS	0	—	—	UC_{DC}	0.54	—
B1-4	30	GDS	100	65	55	CC/P	1.0	0.7
B1-5	32	GDS	100	65	55	CC/P	1.0	0.7
B1-6	35	GDS	400	65	55	CC/P	2.1	1.2
B1-7	57	GDS	400	65	55	CC/P	1.7	1.2
B1-8	65	GDS	900	65	55	CC/P	4.1	2.86
B2-1	28	A	0	—	—	UC_{SC}	0.96	—
B2-2	28	A	0	—	—	UC_{SC}	0.93	—
B2-3	28	GDS	0	—	—	UC_{DS}	0.97	—
B2-4	37	GDS	100	65	55	CC/P	1.3	0.84
B2-5	39	GDS	100	65	55	CC/P	1.2	0.84
B2-6	41	GDS	400	65	55	CC/P	2.6	1.7
B2-7	45	GDS	400	65	55	CC/P	2.5	1.7
B2-8	59	GDS	400	—	—	Confirmation	1.7‡	—
B2-9	61	GDS	900	65	55	CC/P	4.6	3.3
B3-1	28	A	0	—	—	UC_{SC}	2.4	—
B3-2	28	A	0	—	—	UC_{SC}	2.5	—
B3-3	28	GDS	0	—	—	UC_{DS}	2.5	—
B3-4	47	GDS	100	65	55	CC/P	3.1	2.1
B3-5	49	GDS	100	65	55	CC/P	2.9	2.1
B3-6	51	GDS	400	65	55	CC/P	3.4	2.2
B3-7	55	GDS	400	65	55	CC/P	3.2	2.2
B3-8	57	GDS	900	65	55	CC/P	5.2	3.4
B3-9	63	GDS	900	—	—	Confirmation	5.5	3.2

Note: A, Avery compression machine; GDS, Global Digital Systems triaxial apparatus; UC, unconfined compression (subscripts SC and DS represent sulfur-capped and diamond saw–cut end treatments, respectively); CC/P, compression with permeation.
*Specimens are labeled using batch–specimen number.
†Time of testing after mixing.
‡Compressed at a constant rate of 0.001 mm/min.

Table 3. Comparison of local and global strain measurements in GDS apparatus (f_{cu} = 8.3 MPa).

Load (kN)	Local strain (%)	Global strain (%)
5	0.03	0.03
10	0.09	0.09
15	0.17	0.17
20	0.28	0.29
25	0.38	0.41

wall situated below a 30 m high zoned embankment dam founded on a 50 m deep deposit of cohesionless soil. Full details of the finite element analyses can be found in Weck (2007).

Preliminary tests performed with combined compression and permeation indicated the need to eliminate sidewall leakage during compression. This was done by coating the PL-C specimens with a layer of Na–bentonite as described next. First, the cured PL-C specimens were cut with a diamond blade rock saw to achieve flat orthogonal ends and a

10 mm wide strip of filter paper was wrapped around each end of the specimen as shown in Fig. 4. Then, Na–bentonite was mixed at a water content of 62.5% and kneaded until a smooth and consistent material was achieved. The Na–bentonite was applied to the sides of the PL-C specimen and kneaded by hand to minimize air voids. The composite specimen (PL-C plus Na–bentonite) was placed on a 100 mm sample lathe and a wire trimmer was used to remove excess bentonite. Figure 4 shows the final composite specimen, which had a diameter of 100 mm (75 mm diameter PL-C cylinder and 12.5 mm thick Na–bentonite annulus) and height of 150 mm. The 10 mm wide filter paper strips noted above were required to prevent squeezing of the bentonite annulus into the filter stones at the specimen ends during application of high confining stresses.

The composite specimen was placed on a 100 mm diameter base pedestal fitted with an aluminum cap, porous stone, and filter paper disc. Then, a 100 mm diameter filter paper disc, porous stone, and aluminum top cap were placed on top of the specimen. Both top and bottom aluminum caps were modified with additional radial and circumferential grooves to improve drainage from the specimen ends. The resultant hydraulic conductivity of the apparatus was greater than 10^{-3} cm/s.

Two latex membranes were placed over the specimen: first a 70 mm diameter membrane and then a 100 mm diameter membrane. The 70 mm diameter latex membrane was applied using a standard membrane stretcher and sealed to the top cap and base pedestal using two O-rings at each end. The 70 mm membrane was folded back over the O-rings and a bead of silicone caulking was applied along the membrane-to-pedestal and membrane-to-top cap contacts. The 100 mm latex membrane was placed over the 70 mm membrane and sealed at its ends using two O-rings and a bead of silicone caulking identical to that described above for the 70 mm membrane.

Before applying axial load to the PL-C specimen, the bentonite annulus was consolidated using a cell pressure of 1 MPa and a back pressure of 55 kPa for 12, 24, and 36 h for tests performed at confining stresses of 100, 400, and 900 kPa, respectively. This was done to lower the hydraulic conductivity of the Na–bentonite to less than 1×10^{-10} cm/s, which is two orders of magnitude lower than that of the intact PL-C. After consolidating the Na–bentonite, the cell pressure was reduced to the desired confining stress for each test and the top cap and bottom cap pressures were set at 65 and 55 kPa, respectively, and maintained for sufficient time to allow the inflow and outflow to equilibrate. Once the inflow and outflow were equal, the initial hydraulic conductivity of the intact PL-C could be estimated as leakage through the bentonite annulus was less than 1% of the total leakage. It is noted that top and bottom cap pressures were applied using computer-controlled hydraulic actuators, which give precise regulation and measurement of water pressure and volume change. In addition, a confirmatory test was done by consolidating specimen B2-8 using a cell pressure of 400 kPa and back pressure of 55 kPa and waiting for 100% consolidation of the bentonite annulus to occur before compressing the specimen. In all cases, the consolidation response of the bentonite was used to confirm its low hydraulic conductivity compared with that of the PL-C (see Weck 2007).

After following the above procedure, each specimen was loaded in compression at a constant rate of 0.012 mm/min unless otherwise noted. An LVDT was mounted on the load frame so that it came to rest on the triaxial cell and ε_a was deduced from the relative displacement between the load frame and triaxial cell. For each test, the loading was halted at axial strains of 0.5%, 1%, 2%, 4%, 6%, 8%, and 10% and the strain was held constant to measure the hydraulic conductivity. At each strain level, water was permeated through the specimen for at least 8 h using a hydraulic gradient of 6.5, which is comparable to that expected in situ during the service life of a PL-C cut-off wall. Typically, each time the strain was increased it took 5 h for inflow to equilibrate with the outflow due to volume increase (dilatancy) during compression. Thus, the hydraulic conductivity was deduced from the last 3 h of each 8 h permeation stage.

Time-dependent response of PL-C

Significant stress relaxation occurred during the permeation stages of the triaxial compression tests described above. The stress relaxation resulted in a time-dependent reduction of axial stress with time at constant axial strain. To investigate this further, one relaxation test was done (B3-9) without permeation and a second compression test (B2-8) was done without permeation at a compression rate (0.001 mm/min) that was lower than that used in the other tests (0.012 mm/min).

Volume change during compression

Volume change (increase) consistently occurred during compression at axial strains greater than or equal to 0.5%. The volume change can be attributed to dilation of fractures that developed in the specimens for loads causing yield and failure in the PL-C. The volume change manifested as deviations from the inflow-equal-to-outflow condition. Figure 5 shows typical inflow versus outflow response. As noted above, inflow and outflow were measured using computer-controlled hydraulic actuators for precise regulation of top and bottom cap pressures and measurement of volume change. Referring to Fig. 5, increased compression from 1% to 2% strain, for example, resulted in additional water flowing into the specimen rather than through the specimen. Eventually, with time the inflow and outflow would equilibrate after which the hydraulic conductivity could be determined. The volume of water entering the specimen during each strain increment was recorded and divided by the initial specimen volume to deduce the volumetric strain, which is reported below.

Results

Deformation and strength characteristics

Figures 6–8 summarize the stress–strain response of all PL-C specimens during combined permeation and confined compression tests. Figures 7 and 8, however, illustrate typical behaviour for the purpose of discussion.

Referring to Fig. 7, the response of the 0.95 MPa (f_{cu}) PL-C is comparable to that typically observed for clay specimens (e.g., Silvestri et al. 1988). During compression at 0.012 mm/min, the stress–strain response exhibits strain-hardening behaviour. However, during the 8 h periods where the strain was held constant, the axial stress reduced with

Fig. 4. Details of plastic concrete specimens: (*a*) drawings; (*b*) photograph – side view; (*c*) photograph – top view.

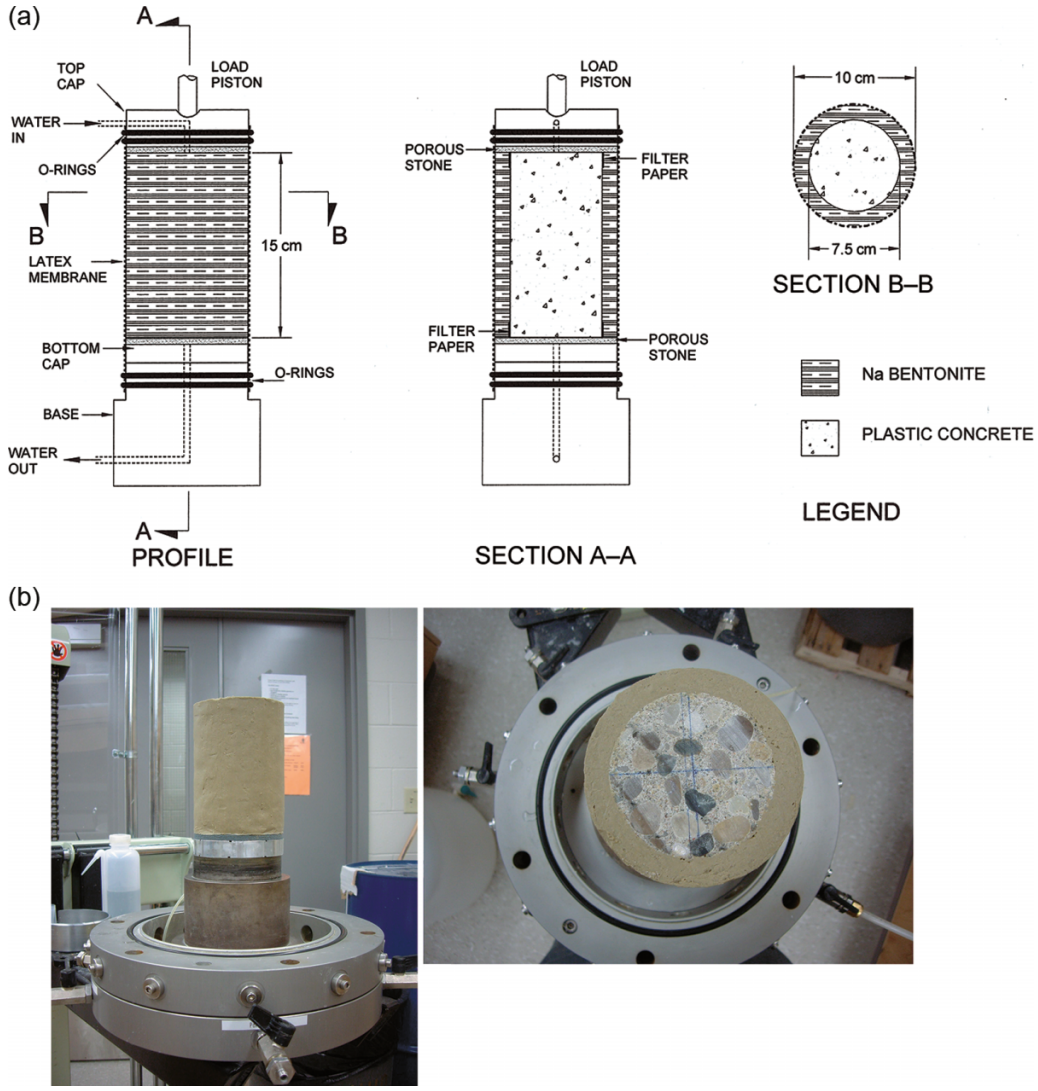

time as illustrated by the data labeled SR_{8hr} in Figs. 7 and 8. From the data shown in Fig. 7, upper bound and lower bound compression curves can be deduced. The upper curve denotes the stress–strain response at a compression rate of 0.012 mm/min, while the lower curve denotes the 8 h relaxed stress–strain response.

For comparison purposes, the stress–strain response of 0.95 MPa (f_{cu}) PL-C during a compression test performed at a constant rate of 0.001 mm/min (specimen B2-8) is also shown in Fig. 7. This test, which was undertaken in the absence of permeation, confirms the sensitivity of plastic concrete to compression rate and it suggests that the 8 h relaxed stress–strain curve is roughly equivalent to that obtained at a slower strain rate of 0.001 mm/min.

Figure 8 shows similar stress–strain response for 2.5 MPa (f_{cu}) PL-C corresponding to a confining pressure of 900 kPa. Again, upper and lower stress–strain curves can be deduced for the 2.5 MPa PL-C specimens. Referring to Fig. 8 and Table 2, it can also be seen that similar results were obtained with or without permeation (see specimens B3-8 and B3-9). Table 2 summarizes the PL-C specimen strength at a compression rate of 0.012 mm/m and the strength deduced after 8 h of relaxation, which is labeled the relaxed strength. On average, the relaxed strength is about 33% lower than that measured at 0.012 mm/min.

Figures 9 and 10 summarize the axial stress versus log-time response of 0.95 MPa (f_{cu}) and 2.5 MPa (f_{cu}) specimens during each of the stress relaxation stages labeled SR_{8hr} in Figs. 7 and 8. From the stress-relaxation response, it can be seen that the relaxation process does not appear to stabilize after the 8 h and as such, the long-term strength of PL-C is likely to be lower than observed in this study and as denoted by the relaxed curves.

Figure 11 shows the normalized compressive strength ($\sqrt{3}\tau_{oct}/f_{cu}$) of PL-C versus normalized mean stress, ($\sqrt{3}\sigma_{oct}/f_{cu}$) from tests performed at a compression rate of 0.012 mm/min. In addition, strength data for normal strength concrete (Seow and Swaddiwudhipong 2005) is also plotted in this figure, where

$$\tau_{oct} = \sqrt{1/2[(\sigma_1 - \sigma_2)^2 + (\sigma_2 - \sigma_3)^2 + (\sigma_3 - \sigma_1)^2]}$$

is the octahedral shear stress at failure, $\sigma_{oct} = (\sigma_1 + \sigma_2 + \sigma_3)/3$ is the octahedral normal stress at failure, and σ_1, σ_2, and σ_3

Fig. 5. Typical volume in and out during triaxial tests with permeation: (*a*) full test; (*b*) response during compression from 1% to 2% axial strain, ε.

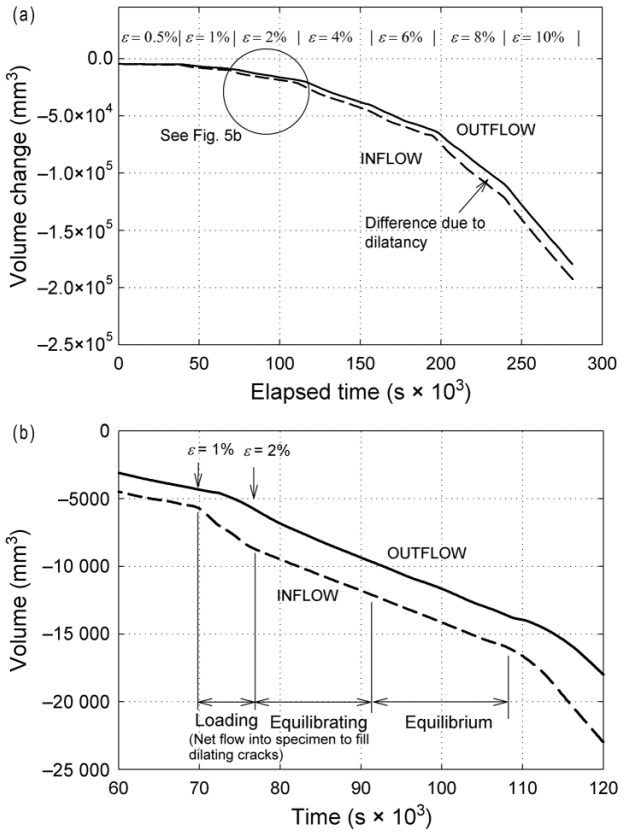

Fig. 6. Summary of stress–strain and stress-relaxation response of plastic concrete.

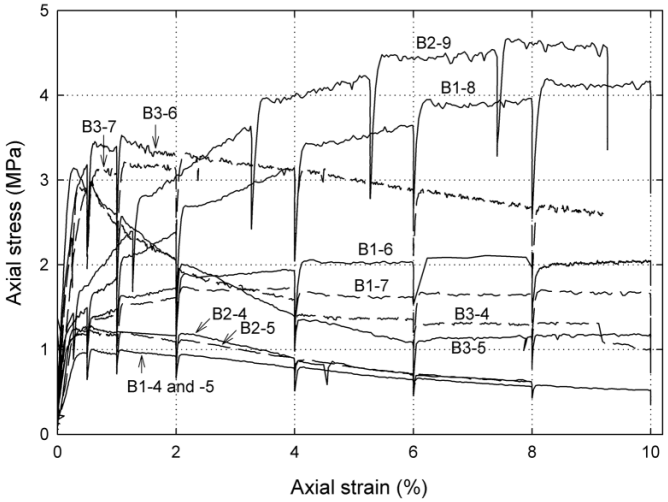

are the major, intermediate, and minor principle stresses, respectively. Figure 11 shows that the variation of PL-C compressive strength versus confining pressure is comparable to that of normal strength concrete. Thus, the failure criteria for normal strength concrete (e.g., Seow and Swaddiwudhipong 2005; Hinchberger 2009) appear to be suitable for PL-C, at least in compression.

Fig. 7. Stress–strain response of 0.95 MPa (f_{cu}) plastic concrete (σ_c = 400 kPa).

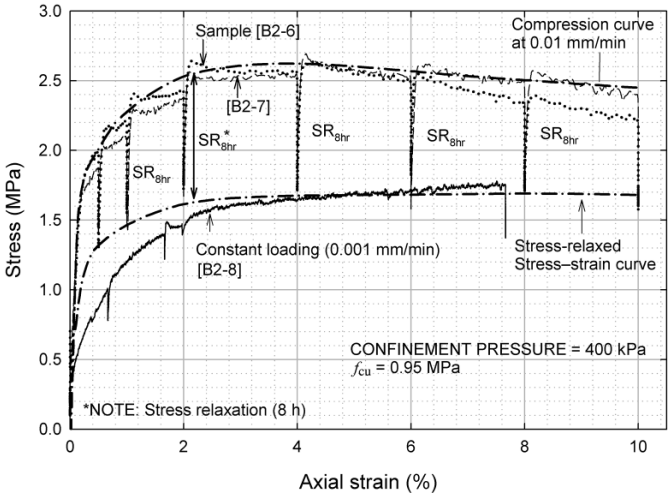

Fig. 8. Stress–strain response of 2.5 MPa (f_{cu}) plastic concrete (σ_c = 900 kPa).

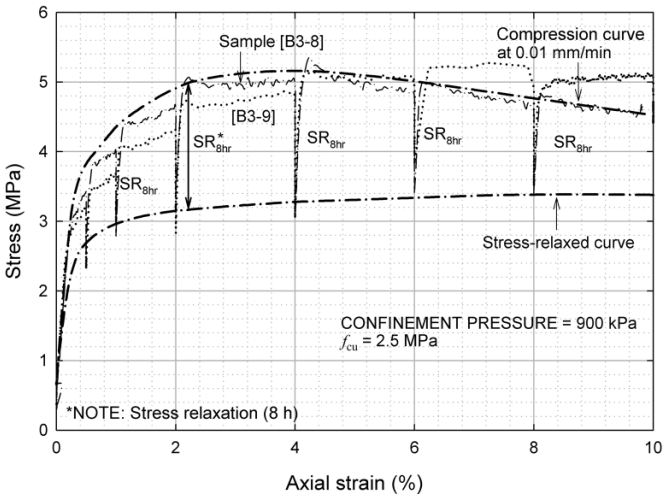

Fig. 9. Stress relaxation versus log-time response of 0.95 MPa (f_{cu}) plastic concrete (σ_c = 400 kPa).

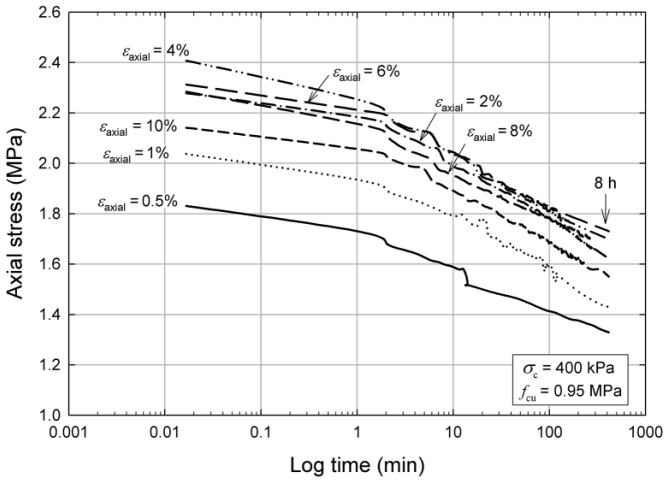

Fig. 10. Stress relaxation versus log-time response of 2.5 MPa (f_{cu}) plastic concrete (σ_c = 900 kPa).

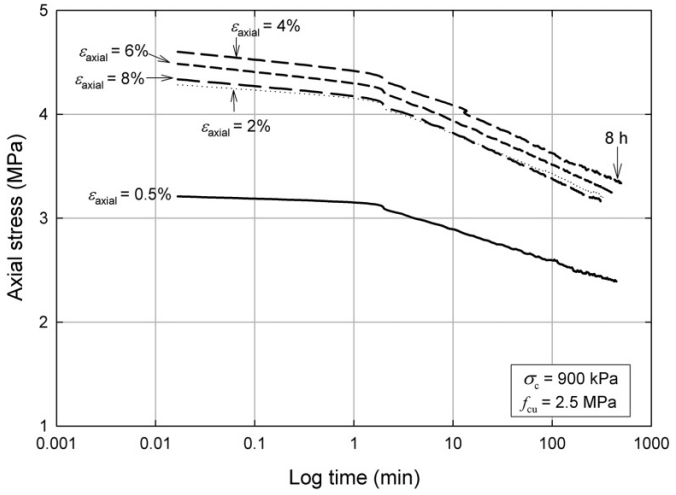

Fig. 11. Comparison of the compressive strength of plastic concrete with normal strength concrete.

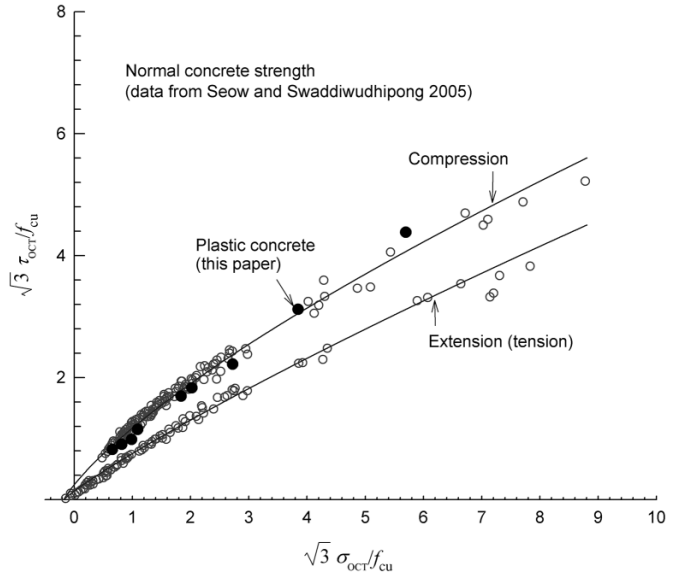

The ratio of elastic modulus to unconfined compressive strength, E/f_{cu}, is summarized in Fig. 12. Overall, the stiffness of the 0.6 MPa (f_{cu}) and 0.95 MPa (f_{cu}) PL-C is strongly influenced by σ_c as shown in this figure. The E/f_{cu} ratio of both the 0.6 and 0.95 MPa specimens roughly doubles as σ_c is increased from the unconfined state to σ_c = 900 kPa. To put this into context, σ_c typically has a strong influence on the elastic modulus, E, of soils (e.g., Janbu 1963). For the 2.5 MPa PL-C specimens, however, there is a change in behaviour. The influence of σ_c on the E/f_{cu} ratio of the 2.5 MPa PL-C is quite small and more comparable to that normally observed for conventional concrete (see Scott et al. 1982). It is noted that the Janbu (1963) parameters for the 0.6 and 0.95 MPa (f_{cu}) PL-C mixes are also presented in Fig. 12.

Lastly, Fig. 13 summarizes the volumetric response of PL-C during triaxial compression and the corresponding

Fig. 12. Modulus ratio (E/f_{cu}) of plastic concrete versus confinement pressure. p_a, atmospheric pressure.

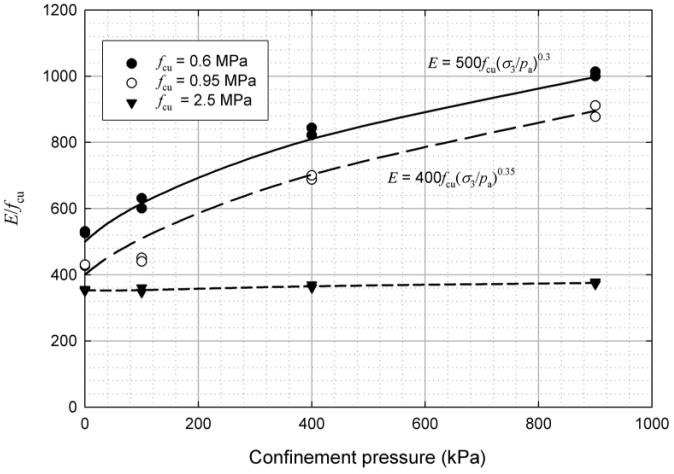

Fig. 13. Volumetric strain versus axial strain.

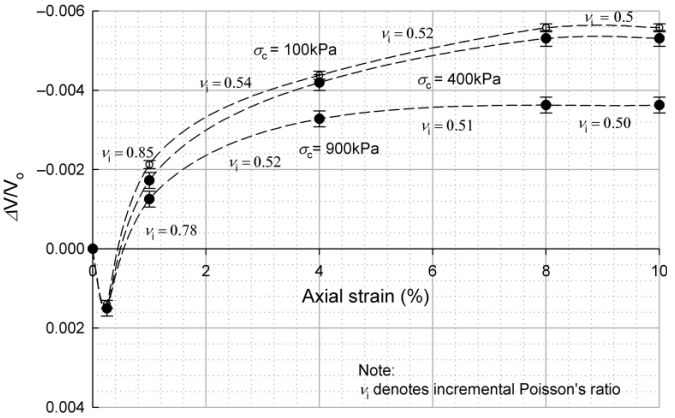

tangent incremental Poisson's ratio (ν_i). The tangent ν_i is shown in this figure as nonlinear elastic constitutive models are often employed in practice to model the response of PL-C. Based on Fig. 13, the following observations can be made. First, all specimens underwent initial volumetric contraction followed by volumetric expansion, which is attributed to yielding and dilation (note that compression is positive). Second, the magnitude of volumetric expansion at failure decreases with increasing σ_c, which is consistent with that observed for normal strength concrete (e.g., Montoya 2003). Third, ν_i increases from about 0.2 to 0.95 immediately after reaching the peak strength, which is indicative of volumetric expansion due to the formation of rough irregular-shaped cracks in the specimens after yield followed by dilation of these cracks with continued compression. Such dilation causes an increase in the crack volume. Finally, ν_i decreases to 0.5 at axial strains in excess of 6%, which corresponds to the constant volume state. Generally, the volumetric response of PL-C during triaxial compression is similar to that observed for other frictional materials. In the following sections, it will be shown that the dilatant behaviour depicted in Fig. 13 leads to comparable variations in the hydraulic conductivity with axial strain.

Fig. 14. Axial strain and hydraulic conductivity of plastic concrete (σ_c = 100 kPa).

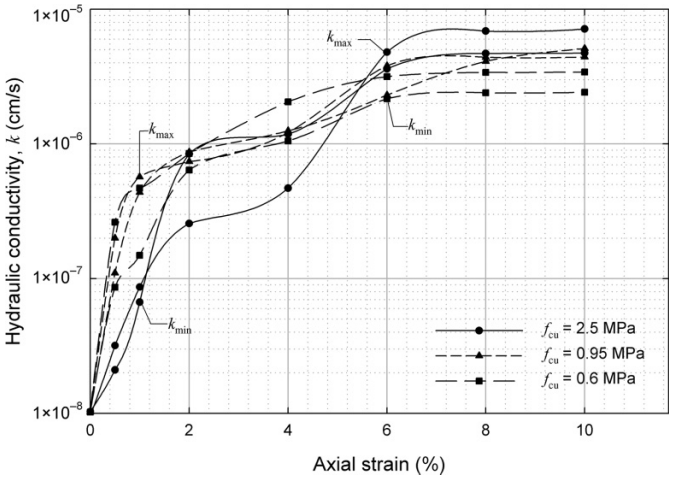

Fig. 15. Axial strain and hydraulic conductivity of plastic concrete (σ_c = 400 kPa).

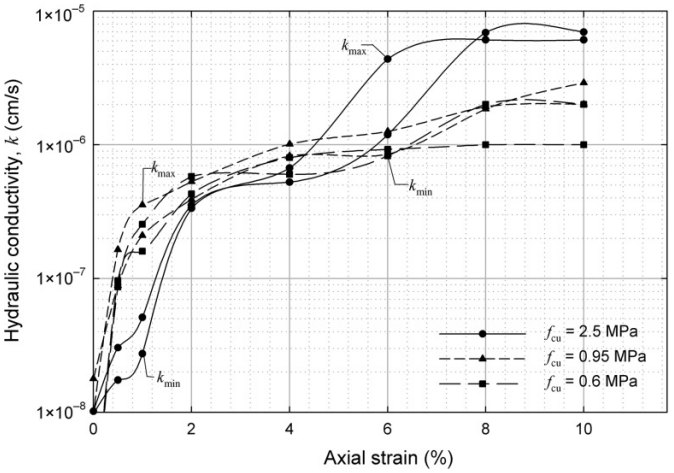

Hydraulic conductivity

Low confinement (σ_c = 100 kPa)

Figure 14 shows the impact of axial strain on the hydraulic conductivity of PL-C at 100 kPa confining stress. Although there is some variation in the test results, it can be seen that there is a consistent trend of increasing hydraulic conductivity with increasing axial strain and dilatancy (see Fig. 13). For most specimens, the hydraulic conductivity increased from the intact value of 1×10^{-8} cm/s to between 3.5×10^{-7} and 7.0×10^{-7} cm/s at 1% axial strain. There is a further increase in the hydraulic conductivity to between 3.5×10^{-6} and 6.0×10^{-6} cm/s for axial strains in excess of about 6%. Considering the intact hydraulic conductivity of PL-C (1×10^{-8} cm/s), these increases are significant and may affect the performance and interpretation of the hydraulic efficiency of PL-C cut-off walls at low confining stresses. The impact of the specimen failure mode on these results will be discussed below.

Intermediate confinement (σ_c = 400 kPa)

Figure 15 shows the effect of axial strain on the hydraulic conductivity of PL-C at 400 kPa confining stress, which is comparable to the stresses expected in the upper portions of cut-off walls below embankment dams between 30 and 50 m in height (see Weck 2007). Similar to that observed at low confining stress, there is a comparable increase in hydraulic conductivity versus increasing axial strain. The hydraulic conductivity increases from 1×10^{-8} cm/s for the intact specimens to between 1.8×10^{-7} and 5.0×10^{-7} cm/s for 0.6 and 0.95 MPa specimens at 1% axial strain. It is interesting that the hydraulic conductivity of 2.5 MPa PL-C increased less than that observed for 0.6 and 0.95 MPa mixes with values ranging from 3×10^{-8} to 9×10^{-8} cm/s at 1% axial strain. The higher strength PL-C appears to be somewhat more resistant to increases in hydraulic conductivity during compressive straining, possibly due to reduced dilatancy. For axial strains in excess of 6%, the hydraulic conductivity is consistently higher than 9×10^{-7} cm/s for all specimens regardless of the compressive strength.

Fig. 16. Axial strain and hydraulic conductivity of plastic concrete (σ_c = 900 kPa).

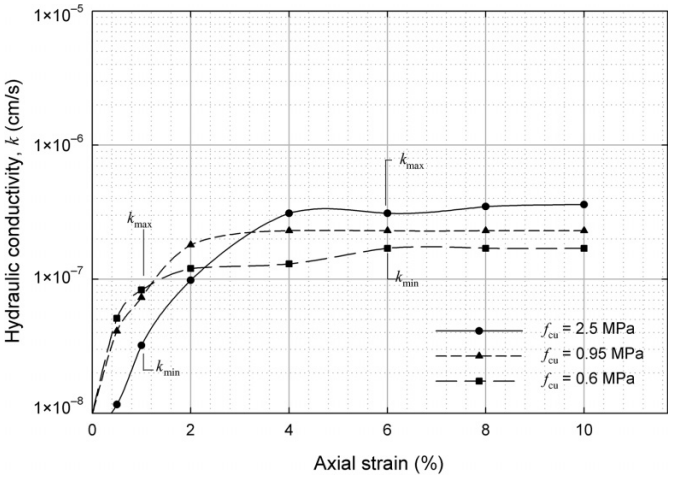

High confinement (σ_c = 900 kPa)

Lastly, the effect of axial strain at high confining stresses (σ_c = 900 kPa) is summarized in Fig. 16 for PL-C with f_{cu} of 0.6, 0.95, and 2.5 MPa. For all tests undertaken at a confining stress of 900 kPa, the increase in hydraulic conductivity during compression is substantially less than observed at lower confining stresses. This is consistent with the lower degree of dilation observed for the results in Fig. 13 corresponding to σ_c = 900 kPa. As shown in Fig. 16, based on three tests, the hydraulic conductivity was found to vary from 3×10^{-8} to 8×10^{-8} cm/s at 1% axial strain. For axial strains in excess of 6%, the hydraulic conductivity was consistently between 1.5×10^{-7} and 3.1×10^{-7} cm/s. Thus, it appears that confining stress in the order of 900 kPa is required to improve the hydraulic response of PL-C subject to large straining. As noted above, the volumetric response of PL-C during compression (see Fig. 13) is consistent with the behaviour depicted in Figs. 14, 15, and 16.

Discussion

Figure 17 summarizes the typical crack patterns recorded at the conclusion of each test corresponding to 10% axial

Fig. 17. Crack patterns for (*a*) low confinement (100 kPa), (*b*) intermediate confinement (400 kPa), and (*c*) high confinement (900 kPa) stresses.

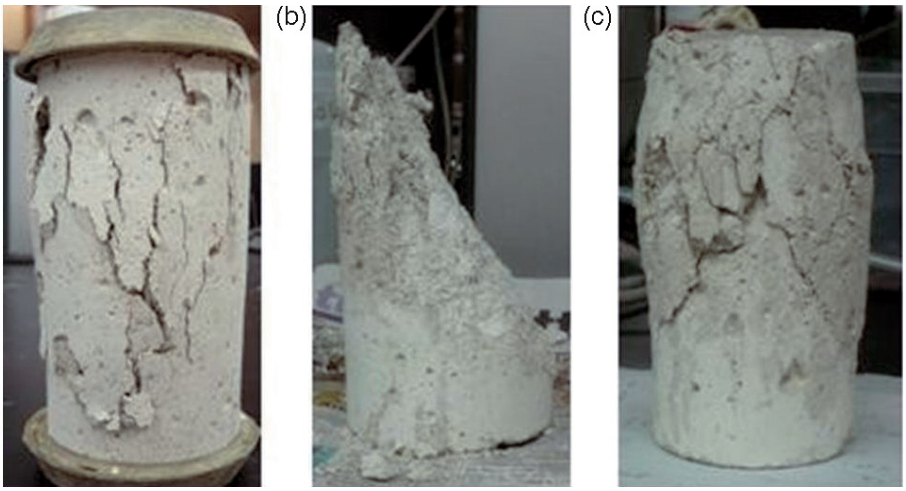

strain. For fractured media, engineering properties are often strongly influenced by specimen size and scale effects. As such, to some extent the results presented in this paper should be considered as a first approximation of the in situ behaviour of PL-C.

Referring to Fig. 17*a*, the predominant crack pattern observed at low confining pressure (100 kPa) was extensive cracking parallel to the specimen axis accompanied by a general shear failure or bulging of the specimen. For these conditions, the crack size was generally much smaller than the specimen size. Consequently, scale effects are considered to have the smallest impact on hydraulic conductivity measurements in Fig. 14 at low confinement.

The failure mode at 400 kPa confining pressure consistently comprised a well-defined failure plane as shown in Fig. 17*b*. As such, it is expected that the results presented in Fig. 15 corresponding to a σ_c of 400 kPa are probably influenced by scale effects and thus, represent semiquantitative changes in the hydraulic conductivity of the PL-C. Nonetheless, the results illustrate two characteristics: (*i*) the effective hydraulic conductivity of PL-C is adversely affected by axial strain at intermediate confining stresses, and (*ii*) 2.5 MPa (f_{cu}) PL-C appears to be more resistant to increases in hydraulic conductivity, at least for axial strains up to 1%.

To conclude, from Fig. 17*c*, a mixed failure mode comprising cracking parallel to the specimen axis and a well-defined failure plane was typically observed for compression tests at a σ_c of 900 kPa. Consequently, scale effects are expected to impact these results as well, but to a lesser extent than that observed at σ_c = 400kPa.

Summary and conclusions

In summary, this paper has described a laboratory investigation into the mechanical and hydraulic characteristics of PL-C subjected to triaxial compression for confining pressures ranging from unconfined to 900 kPa. In addition, the effect of compression and strain on the hydraulic conductivity of PL-C has been evaluated using a triaxial apparatus capable of compression and simultaneous permeation and specimens prepared with an annulus of bentonite to control sidewall leakage. Based on the results of this study, the following conclusions may be drawn:

(1) The stress–strain response of PL-C is strongly influenced by the rate of loading and time effects such as stress relaxation. It was found that the strength of PL-C typically dropped by 33% after 8 h of relaxation, similar to that seen for clayey soils. As such, it is concluded that a time-dependent constitutive model is required to predict the in situ working strains in a PL-C cut-off wall subject to loads from an embankment dam. The use of a time-independent model for this material may lead to underestimation of the long-term working strains.

(2) The normalized compressive strength of PL-C versus confining pressure is comparable to that of normal strength concrete as shown in Fig. 11. Thus, it is concluded that failure criteria used for concrete should be suitable for PL-C in compression.

(3) The modulus of elasticity of PL-C is strongly influenced by σ_c for 0.6 and 0.95 MPa (f_{cu}) mixes. Analogous behaviour has been observed in soils and Janbu's equation (Janbu 1963) provides a reasonable fit for the observed behaviour. It is also noted that the Janbu parameters provided in Fig. 12 of this paper could be considered when using numerical models to assess the effect of embankment construction on PL-C cut-off walls.

(4) Variations in the modulus of 2.5 MPa (f_{cu}) PL-C versus σ_c were more comparable to that observed for concrete (e.g., Scott et al. 1982) indicating that a pressure dependent elastic model may not be required for modeling cut-off walls with high-strength PL-C below embankment dams.

(5) As shown in this study, the hydraulic conductivity of PL-C increases significantly with compression and consequent axial straining, due to crack formation and dilation of cracks. Although some of the laboratory results are affected by scale effects, the results are considered to be a reasonable first approximation of behaviour. If a strain-based design criterion is adopted for a PL-C cut-off wall, then results such as those presented in

Figs. 14–16 should provide a basis for developing a suitable working-strain limit.

(6) Mahboubi and Ajorloo (2004) have shown that PL-C has lower porosity, lower intact permeability, and a higher elastic modulus when it is cured at high σ_c compared with no confinement as done in this study. As such, it should be noted that the stiffness and intact permeability of the PL-C tested in the current study are likely lower and higher, respectively, than the corresponding material cured in situ where the confining pressures are significant. However, the post-yield dilation of PL-C and the resultant increase in hydraulic conductivity is probably not that sensitive to the stress state during curing as this behaviour is governed by the geometry and roughness of cracks that develop after yield and failure, which is dictated by the aggregate.

(7) Finally, the tests performed in this study indicate that rough irregular cracks form in PL-C after yielding in compression in spite of its ductility relative to normal strength cement. Depending on the axial strain induced by dam construction, significant cracking and dilation could occur resulting in increased hydraulic conductivity, which is independent of the PL-C strength. The crack patterns observed in this study suggest that leakage through such a material would follow tortuous flow paths, which could increase the likelihood of hydraulic erosion (Davidson et al. 1992). As such, mix designs that are more resistant to hydraulic erosion should be considered for situations where high strains are expected and the head across the cut-off wall is high.

Acknowledgements

The research presented in this paper has been undertaken with Discovery Grants awarded to Drs. S. Hinchberger and T.A. Newson by the Natural Sciences and Engineering Research Council of Canada. The authors would also like to acknowledge the financial support and assistance of Dr. Rob Dawson (Hatch Ltd.) over the course of this investigation.

References

ASTM. 1998*a*. Standard test method for slump of hydraulic-cement concrete. ASTM standard C143. Annual Book of ASTM Standards. American Society for Testing and Materials, West Conshohocken, Pa.

ASTM. 1998*b*. Standard practice for capping cylindrical concrete specimens. ASTM standard C617. American Society for Testing and Materials, West Conshohocken, Pa.

ASTM. 2005. Standard test methods for laboratory determination of water (moisture) content of soil and rock by mass. ASTM standard D2216. American Society for Testing and Materials, West Conshohocken, Pa.

Balian, S. 2007. Cut-off wall construction (Peribonka Dam). International Water Power and Dam Construction, **59**(2): 42–44.

Davidson, R.R., Levallois, J., and Graybeal, K. 1992. Seepage cutoff walls for mud mountain dam. *In* Slurry walls: design, construction, and quality control. ASTM Special Technical Publication No. 1129. American Society for Testing and Materials, Philadelphia, Pa. pp. 309–323.

Hinchberger, S.D. 2009. A simple single-surface failure criterion for concrete. Journal of Engineering Mechanics, **135**(7): 729–732. doi:10.1061/(ASCE)0733-9399(2009)135:7(729).

Hutchinson, M.T., Daw, G.P., Shotton, P.G., and James, A.N. 1975. The properties of bentonite slurries used in diaphragm walls and their control. *In* Diaphragm Walls and Anchorage, Proceedings of the Conference organized by the Institution of Civil Engineers, London, England, 18–20 September 1974. Institution of Civil Engineers, London. pp. 33–39.

Issa, S.A., Islam, M.A., Issa, M.A., Youssif, A.A., and Issa, M.A. 2000. Specimen and aggregate size effect on concrete compressive strength. Journal of Cement, Concrete and Aggregates, **22**(2): 103–115. doi:10.1520/CCA10470J.

Janbu, N. 1963. Soil compressibility as determined by oedometer and triaxial tests. *In* Proceedings of the European Conference on Soil Mechanics and Foundation Engineering, Weisbaden, Germany, 15–18 October 1963. Deutsche Gesellschaft für Erd- und Grundbau, Essen, Germany. Vol. 1, pp. 19–25.

Kahl, T., Kauschinger, J.L., and Perry, E.B. 1991. Plastic concrete cutoff walls for earth dams. U.S. Army Engineering Waterways Experimental Station, Vicksburg, Miss.

Mahboubi, A., and Ajorloo, A. 2004. Experimental study of the mechanical behavior of plastic concrete in triaxial compression. Cement and Concrete Research, **35**(2): 412–419. doi:10.1016/j.cemconres.2004.09.011.

Menzies, B. 1988. A computer controlled hydraulic triaxial testing system. *In* Advanced triaxial testing of soil and rock. ASTM STP 977. *Edited by* R.T. Donaghe, R.C. Chaney, and M.L. Silver. American Society for Testing and Materials (ASTM), Philadelphia, Pa. pp. 82–94.

Montoya, E. 2003. Behaviour and analysis of confined concrete. Ph.D. thesis, University of Toronto, Toronto, Ont.

Rigbey, S. 2006. Shikwamkwa dam replacement project. *In* Proceedings of the Hatch Energy Symposium on Dams, Niagara Falls, Ont., 18 April 2006. [CD-ROM]. Hatch Ltd., Niagara Falls, Ont.

Scott, B.D., Park, R., and Priestley, M.J. 1982. Stress-strain behaviour of concrete confined by overlapping hoops at low and high strain rates. ACI Journal, **79**(2): 13–27.

Seow, P., and Swaddiwudhipong, S. 2005. Failure surface for concrete under multiaxial load — a unified approach. Journal of Materials in Civil Engineering, **17**(2): 219–228. doi:10.1061/(ASCE)0899-1561(2005)17:2(219).

Silvestri, V., Soulie, M., Touchan, Z., and Fay, B. 1988. Triaxial relaxation tests on a soft clay. *In* Advanced triaxial testing of soil and rock. ASTM STP 977. *Edited by* R.T. Donaghe, R.C. Chaney, and M.L. Silver. American Society for Testing and Materials, Philadelphia, Pa. pp. 321–337.

Soroush, A., and Soroush, M. 2005. Parameters affecting the thickness of bentonite cake in cutoff wall construction: case study and physical modeling. Canadian Geotechnical Journal, **42**(2): 646–654. doi:10.1139/t04-090.

Weck, J.V. 2007. Mechanical and hydraulic characterization of plastic concrete. M.E.Sc. thesis, The University of Western Ontario, London, Ont.